PII: S1043-6618(20)31604-2

DOI: https://doi.org/10.1016/j.phrs.2020.105296

Reference: YPHRS 105296

To appear in: *Pharmacological Research*

Received Date: 16 August 2020

Revised Date: 3 November 2020

Accepted Date: 4 November 2020

Discovery of a novel short peptide with efficacy in accelerating the healing of skin wounds

Ying Wang[2, #], Zhuo Feng[1, #], Meifeng Yang[1, #], Lin Zeng[4, #], Bu'er Qi[1], Saige Yin[1], Bangsheng Li[3], Yilin Li[1], Zhe Fu[1], Longjun Shu[2], Chen Fu[1], Pan Qin[1], Yi Meng[1], Xiaojie Li[3], Ying Yang[5], Jing Tang[3, *] gracett916@163.com, Xinwang Yang[1, *] yangxinwanghp@163.com

[1]Department of Anatomy and Histology & Embryology, Faculty of Basic Medical Science, Kunming Medical University, Kunming, Yunnan, China, 650500.

[2]Key Laboratory of Chemistry in Ethnic Medicine Resource, State Ethnic Affairs Commission & Ministry of Education, School of Ethno-Medicine and Ethno-Pharmacy, Yunnan Minzu University, Kunming, Yunnan, China, 650504.

[3]Department of Biochemistry and Molecular Biology, Faculty of Basic Medical Science, Kunming Medical University, Kunming, Yunnan, China, 650500.

[4]Public Technical Service Center, Kunming Institute of Zoology, Chinese Academy of Sciences, Kunming, Yunnan, China, 650223.

[5]Department of Endocrinology and Metabolism, Second People's Hospital of Yunnan Province & Fourth Affiliated Hospital of Kunming Medical University, Kunming 650021, Yunnan, China, 650223.

[*]Corresponding authors:

Prof. Xinwang Yang, Faculty of Basic Medical Science, Kunming Medical University, 1168 West Chunrong Road, Kunming, Yunnan, China, 650500. telephone: +86 13577174345.

Prof. Jing Tang, Faculty of Basic Medical Science, Kunming Medical University, 1168 West Chunrong Road, Kunming, Yunnan, China, 650500. telephone: +86 13629600409.

[#] **These authors contributed equally to this work**

Graphical abstract

Abstract

Despite extensive efforts to develop efficacious therapeutic approaches, the treatment of skin wounds remains a considerable clinical challenge. Existing remedies cannot sufficiently meet current needs, so the discovery of novel pro-healing agents is of growing importance. In the

current research, we identified a novel short peptide (named RL-QN15, primary sequence 'QNSYADLWCQFHYMC') from *Rana limnocharis* skin secretions, which accelerated wound healing in mice. Exploration of the underlying mechanisms showed that RL-QN15 activated the MAPK and Smad signaling pathways, and selectively modulated the secretion of cytokines from macrophages. This resulted in the proliferation and migration of skin cells and dynamic regulation of TGF-β1 and TGF-β3 in wounds, which accelerated re-epithelialization and granulation tissue formation and thus skin regeneration. Moreover, RL-QN15 showed significant therapeutic potency against chronic wounds, skin fibrosis, and oral ulcers. Our results highlight frog skin secretions as a potential treasure trove of bioactive peptides with healing activity. The novel peptide (RL-QN15) identified in this research shows considerable capacity as a candidate for the development of novel pro-healing agents.

Chemical compounds: Lipopolysaccharide (PubChem CID: 75107052); Streptozotocin (PubChem CID: 29327); Exendin-4 (PubChem CID: 45588096); Pentobarbital sodium: (PubChem CID: 23676152); Acetic Acid: (PubChem CID: 176); Bleomycin: (PubChem CID: 5360373).

Abbreviations: HaCaT, human keratinocytes; DM, diabetes mellitus; H&E, Hematoxylin and Eosin; DEGs, Differentially Expressed Genes; GO, Gene Go; KEGG, Kyoto Encyclopedia of Genes and Genomes; MAPKs, Mitogen-Activated Protein Kinase; TGF-β, Transforming Growth Factor-β. TFA, Trifluoroacetic Acid; RP-HPLC, Reversed-phase High-performance Liquid Chromatography; DTT, Dithiothreitol; ACN, Acetonitrile; FBS, Fetal Bovine Serum; TNF-α, Tumor Necrosis Factor; IL, Interleukin; VEGF, Vascular Endothelial Growth Factor; LPS, Lipopolysaccharide; PVDF, Polyvinylidene Fluoride; PBS, Phosphate-Buffered Saline; EGFR, Epidermal Growth Factor Receptor; cAMP, cyclic Adenosine monophosphate; KEGG, Kyoto Encyclopedia of Genes and Genomes; DEG, differentially expressed genes; GO, Gene Ontology; KFX, KangFuXin; STZ, streptozotocin.

Keywords: Wound healing, pro-healing agents, peptide, amphibian, RL-QN15.

1. Introduction

As the largest human organ and physical barrier to the external environment, skin plays an essential role in temperature regulation as well as protection, perception, excretion, absorption, metabolism, and immunity. The structural integrity of the skin is also crucial for the maintenance of physiological functions. However, many insults, including mechanical, thermal, chemical, and radiative stimulation, can lead to skin damage, tissue loss, and structural and functional impairment [1, 2]. After injury, the body usually initiates a series of highly complex and overlapping physiological processes for wound repair: i.e., hemostasis, inflammation, proliferation, and remodeling. Each stage is tightly controlled and includes the regulation of various cells (e.g., fibroblasts, macrophages, platelets, and epithelial keratinocytes) and substances (e.g., fibroblast, platelet-derived, transforming, endothelial, and epidermal growth factors) [3, 4].

Although skin repair is an innate and universal process, various factors can affect the stages of healing, resulting in chronic non-healing wounds or excessive wound healing. Chronic non-healing wounds provide the opportunity for pathogens to invade and reproduce, leading to infection, sepsis, water and electrolyte disorders, multiple organ failure, and secondary diseases, as well as an increase in the physiological and economic burden on patients [5]. Excessive wound healing is often exemplified by hypertrophic scars and keloids, which can affect skin appearance, formation and function [6]. Both excessive wound healing and chronic non-healing wounds impair the normal physiological function of skin, resulting in serious clinical and financial costs [7-9].

Considerable efforts have been expended to investigate effective methods for the healing of skin wounds. Although novel therapies, such as stem cell and tissue engineering technologies, have attracted attention, interventional drug therapy remains crucial [3, 10-12]. At present, the most commonly used clinical drugs include small molecular compounds and growth factors. However, these single-type drugs have several limitations: for example, the former are unstable, difficult to synthesize, and exhibit unsatisfactory activity; the latter require strict preservation conditions and are easily inactivated during transportation, preservation, and use, and more importantly, can cause excessive wound repair, resulting in hypertrophic scars [13-15]. Therefore, in clinical practice, skin wound repair and regeneration still face enormous challenges and existing drugs are unable to meet growing clinical needs. Thus, the identification and development of molecules with strong healing activity and low production costs are essential.

Since 2000, approximately 30 peptide drugs have been approved, with several achieving great success, e.g., abaloparatide, semaglutide, and plecanatide [16]. These peptide drugs demonstrate considerable advantages, including relatively straightforward compound discovery, comparatively high affinity and selectivity with receptors *in vivo*, reasonably high safety, limited toxic metabolites, fast clearance rate, poor accumulation and reduced interactions with other drugs [17, 18]. The success of peptide drug development is much higher than that of small molecular compounds, which has resulted in growing interest worldwide [19-22]. Although remarkable achievements have been made, only a few non-growth factor peptides have shown the ability to increase skin wound repair [23]. While active wound repair peptides with high activity, strong stability, and low cost have broad market prospects, the discovery of drug

candidate molecules remains scarce.

Amphibians are a natural repository of active peptides. Many different active peptides from frog skin secretions, such as Esculentin-1a (1-21) NH_2 and Temporins A and B, are reported to show accelerated wound-healing activity [24-26]. In this study, we identified a novel short pro-healing peptide (named RL-QN15) with an amino acid sequence of 'QNSYADLWCQFHYMC' from *Rana limnocharis* skin secretions. RL-QN15 showed significant therapeutic potency against chronic wounds, skin fibrosis, and oral ulcers. Thus, RL-QN15 exhibits strong potential as a candidate for the development of efficacious skin wound repair agents.

2. Materials and Methods

2.1 Collection of frog skin secretions and animal ethics

Adult *R. limnocharis* frogs (n = 50) were collected in Hekou County, Yunnan Province, China. The frog skins were stimulated for secretion collection, as per previous research [27]. All animal procedures were approved and conducted in accordance with the requirements of the Ethics Committee of Kunming Medical University, Yunnan, China.

2.2 Purification procedure

Lyophilized secretions were re-dissolved in ultrapure water and then centrifuged at 12 000 × *g* for 20 min at 4 °C. The supernatant was collected and ultrafiltered by an Amicon Ultrafilter with a cutoff molecular weight of 10 KDa (Merck-Millipore, Germany). The resulting sample

was then purified by two rounds of reversed-phase high-performance liquid chromatography (RP-HPLC) with a C18 column (Hypersil BDS C18, 4.0 × 300 mm, Elite, China) pre-equilibrated with 0.1% (v/v) trifluoroacetic acid (TFA) in water. Elution was performed using a linear gradient (0%–65% acetonitrile over 65 min) of 0.1% (v/v) TFA in H_2O at a flow rate of 1 mL/min, with monitoring at 220 nm. Fractions with cellular-level wound healing activity were collected, lyophilized, and stored at −20 °C for future use.

2.3 Analysis of peptide primary structure

Samples dissolved in 25 mM NH_4HCO_3 buffer at a final concentration of 0.5 μg/μL were reduced by 10 mM DTT at 37 °C for 40 min. Afterward, 1 μL of the native or reduced peptide was mixed with an equal volume of α-cyano-4-hydroxycinnamic acid (5 mg/ml, dissolved in 50% ACN, 0.1% TFA) and applied to a stainless-steel plate. Following crystallization, the plates were analyzed using a mass spectrometer (Autoflex speed TOF/TOF, Bruker Daltonik GmbH, Leipzig). The MS and MS/MS detection modes were employed to detect molecular weight and sequence information, respectively [27]. Results were also confirmed by Edman degradation on a PPSQ-31A protein sequencer (Shimadzu, Japan) according to the manufacturer's standard GFD protocols. The skin of one adult frog was used for cDNA cloning, RNA extraction, cDNA synthesis, and cDNA encoded peptide screening by polymerase chain reaction (PCR). The sequencing of PCR products was performed as per our previous report [28]. The *de novo* structure of RL-QN15 was predicted using the PEP-FOLD3 online service in accordance with other research [29].

2.4 Peptide synthesis

All peptides with purity higher than 95% used in this research were commercially synthesized by Wuhan Bioyeargene Biotechnology Co. Ltd. (Wuhan, China). The synthesized RL-QN15 was analyzed by mass spectrometry and co-eluted with native RL-QN15 to ensure the correct structure.

2.5 Cellular proliferation, migration, and scratch healing assay against keratinocytes

Immortalized human keratinocytes (HaCaT) were cultured in DMEM/F12 (BI, Israel) supplemented with 10% (v/v) fetal bovine serum (FBS, Hyclone, USA) and antibiotics (100 units/ml penicillin and 100 units/ml streptomycin) at 37 °C in a humidified atmosphere of 5% CO_2. The effects of different concentrations of RL-QN15 on HaCaT cell proliferation were then determined based on previous study [30]. The effects of RL-QN15 on HaCaT cell migration were also tested using a 24-well plate with Falcon cell culture inserts (8-μm pores, Corning, USA) as per previous research [31]. In addition, the effects of RL-QN15 on HaCaT cell scratch healing were determined following an earlier study [32]. The effects of inhibitors of the MAPK signaling pathway, i.e., SB239063, SB600125, and PD98059 (10 μM, MedChemExpress, USA), and TGF-β1/Smad signaling pathway, i.e., ITD-1 (10 μM, Selleck, China), on RL-QN16-induced HaCaT cell migration and scratch healing were also determined [33].

2.6 Effects of RL-QN15 on release of cytokines from macrophages (RAW264.7)

Mouse macrophages (RAW264.7) were cultured in DMEM/F12 (BI, Israel) supplemented with 10% (v/v) FBS (Hyclone, USA) and antibiotics (100 units/ml penicillin and 100 units/ml streptomycin) at 37 °C in a humidified atmosphere of 5% CO_2. The effects of RL-QN15 on RAW264.7 cell proliferation were determined according to prior research [31].

The RAW264.7 cells (1×10^5) were first seeded in a 96-well culture plate for 4 h to ensure adhesion, then incubated with a vehicle or different concentrations of RL-QN15 for 9 h. The supernatants of medium were then collected, and the contents of TNF-α, TGF-β1, IL-1β, IL-6, VEGF (NeoBioscience, Shanghai, China), TGF-β3, and Smad7 (Jianglai Bioscience, Shanghai, China) were detected using ELISA kits following the manufacturer's instructions. To detect TNF-α, the cells were also stimulated using vehicle, lipopolysaccharide (LPS, 1 μg/mL, Sigma-Aldrich, St Louis, MO, USA) from *Escherichia coli*, or LPS (1 μg/mL) and RL-QN15 (combined) at different concentrations. In addition, three MAPK signaling pathway inhibitors, i.e., PD98059, SP600125, and SB203580 (20 μM, MedChemExpress, USA), were co-incubated with RL-QN15 (10 nM) for 9 h, with the contents of TGF-β1 and TGF-β3 in the supernatants of medium then tested.

2.7 Differential transcript expression and bioinformatics analyses

The RAW264.7 cells (5×10^6) were seeded in 6-well culture plates. After adhesion, the cells were cultured in serum-free medium and then incubated with vehicle or RL-QN15 (10 nM) for 2 h, with total RNA then extracted using an RNA extraction kit (Tiangen, Beijing, China). Total RNA (three for vehicle and three for RL-QN15) library construction and transcriptome sequencing were conducted by the BGI Company (Shenzhen, China). The clean reads were compared to the reference gene sequence using Bowtie v2 and the gene expression level of each sample was calculated using RSEM (RNA-Seq by Expectation-Maximization). A DEGseq (differentially expressed genes from RNA-seq) Q-value of <0.05 was considered statistically significant. We used 'GO: TermFinder' (http://www.geneontology.org/) to identify significantly

enriched Gene Ontology (GO) terms and biological functions in candidate genes. Furthermore, we performed KEGG (Kyoto Encyclopedia of Genes and Genomes) pathway analysis (http://www.genome.jp/KEGG/) to determine the most important metabolic and signal transduction pathways in candidate genes, with the top 10 significant pathways (Q-value ≤ 0.05) selected [34].

2.8 Effects of RL-QN15 on regulation of MAPK and Smad signaling pathways

The RAW264.7 cells (5×10^6) were seeded in 6-well culture plates. After adhesion, the cells were cultured in serum-free medium and incubated with vehicle or RL-QN15 at different concentrations for 2 h (MAPK signaling pathway) or 16 h (Smad signaling pathway). Cells were then treated with lysate (RIPA and PMSF, Meilun Biotechnology, Dalian, China; phosphatase inhibitors, Roche, Shanghai, China). The proteins were quantified by the Bradford method (BCA protein analysis kit, Meilun, Dalian, China). Protein samples were then separated by 12% sodium dodecyl sulfate-polyacrylamide gel electrophoresis (SDS-PAGE), electroblotted onto polyvinylidene fluoride (PVDF) membranes, and analyzed by western blotting as per previous study [35]. Primary antibodies, including β-actin, Erk1/2, p-Erk1/2, JNK, p-JNK, P38, p-P38, Smad2, p-Smad2, Smad3, p-Smad3 (Cell Signaling Technology, Danvers, MA, USA), and Smad7 (Bioss, Beijing, China), were used for western blotting following the provided instructions.

2.9 Effects of RL-QN15 on healing of acute full-thickness dorsal skin wounds in mice

Male Kunming mice (22-24 g, five weeks old) were randomly selected to establish acute full-thickness dorsal skin wounds, as per previous research [30]. The wounds were topically treated

with vehicle, Kangfuxin (KFX, 10 mg/mL, ethanol extract of the American cockroach, Inner Mongolia Jingxin Pharmaceutical Co. Ltd., China), or RL-QN15 at different concentrations twice a day. Wound condition was documented, with ImageJ software employed to estimate wound area (percentage of residual wound area to initial area) and GraphPad Prism used to quantify wound healing. Skin tissue samples from the central area of the wounds were taken from mice following topical treatment with vehicle, KFX (10 mg/mL), or RL-QN15 (50 nM) at days 5 and 9 post-surgery. The skin samples were then stained using hematoxylin & eosin (H&E) and analyzed histologically.

2.10 Effects of RL-QN15 on levels of TGF-β1 and TGF-β3 in acute skin wound tissues

Samples from the central area of the acute full-thickness skin wounds were obtained from mice on days 3 and 9 post-surgery, then homogenized in phosphate-buffered saline (PBS; 1:9, weight/volume), and centrifuged at 12 000 × *g* for 20 min at 4 °C. The supernatants were collected and TGF-β1 and TGF-β3 levels were analyzed using ELISA kits (Jianglai Bioscience, Shanghai, China).

2.11 Effects of RL-QN15 on healing of chronic full-thickness dorsal skin wounds induced by diabetes mellitus in mice

Male C57BL/6 mice (20-24 g, 6-8 weeks old) were randomly selected to establish chronic full-thickness dorsal skin wounds. Briefly, the mice were fed high-fat diets for one month and were then injected intraperitoneally with STZ (streptozotocin, 30 mg/kg/d, Sigma-Aldrich, St Louis, MO, USA) for 5 d. The levels of fasting blood glucose were determined by relevant meters (Roche, Basel, Switzerland), and full-thickness dorsal skin wounds were established on

those mice exhibiting diabetes mellitus (fasting blood glucose levels of ≥11.1 mM), as per previous studies [30, 36]. The chronic full-thickness skin wounds induced by diabetes were topically treated with vehicle, exendin-4 (50 nM, Baxter Pharmaceutical Solutions LLC, USA), or RL-QN15 (50 nM) twice a day. Wound condition was documented, with ImageJ employed to estimate wound area (percentage of residual wound area to initial area) and GraphPad Prism used to quantify wound healing rate. Skin tissue samples from the central part of the wounds were taken from mice topically treated with vehicle or RL-QN15 (50 nM) on days 5, 9, and 13 post-surgery. The samples were then stained using H&E and analyzed histologically.

2.12 Effects of RL-QN15 on healing of oral ulcers in rats

The potency of RL-QN15 on the acceleration of oral ulcer healing was examined, as reported previously [37]. Briefly, SD rats (180-200 g, 8-10 weeks old) were anesthetized with a 100-mL intraperitoneal injection of 30% pentobarbital sodium solution (100 μL/100 g). A round filter paper (6 mm in diameter) soaked with 15 μL of 50% acetic acid was then applied over the gum of the lower lip for 60 s, which led to a uniform and circular ulcer. We then topically applied 50 μL of RL-QN15 liquid (10 pM, 100 pM, or 1 nM) on the ulcer in the experimental group twice a day, with 50 μL of saline used in the vehicle group and 50 μL of KFX liquid (10 mg/mL) used as the positive control. Images of oral ulcer healing were taken at 1-d intervals, and the healing rate was calculated using ImageJ and GraphPad Prism software. Tissue samples from the central part of the oral ulcers were taken from rats topically treated with vehicle, KFX (10 mg/mL), or RL-QN15 (10 nM) on days 2 and 7 post-surgery. Samples were then stained using H&E and analyzed histologically.

2.13 Effects of RL-QN15 on skin fibrosis in mice

A skin fibrosis model was produced following prior research [38]. Briefly, female mice aged 8 weeks were randomly selected and grouped into the preventive and curative model groups. The shaved dorsal skins of mice in the preventive model were injected subcutaneously with bleomycin (1 mg/mL, dissolved in saline, 150 μL, Hisun Pfizer Pharmaceuticals Co. Ltd., China) daily, concurrent with RL-QN15 (6 μg/kg, dissolved in saline) for 4 weeks. Subcutaneous injections of saline alone or RL-QN15 (6 μg/kg, dissolved in saline) served as two controls. In the curative model, either bleomycin (1 mg/mL) or saline was injected on alternate days for 6 weeks. Two weeks after the first administration, mice were given a daily dose of RL-QN15 (6 μg/kg, dissolved in saline) or vehicle for the remaining 4 weeks. Finally, the mice in both groups were sacrificed by cervical dislocation. Skin tissue was then removed and stained with H&E and Masson's trichrome for histological analysis.

2.14 Histological analysis

As stated above, tissue samples were stained with either H&E (acute skin wounds, chronic skin wounds, and oral ulcers) or H&E and Masson's trichrome (fibrotic skin wounds) [35]. Dermal thickness in fibrotic skins was defined as the thickness of the skin from the top of the granular layers to the junction between the dermis and subcutaneous fat layer in five distinct fields at an equal magnification (×40) using a light microscope. Fibrotic level was quantified on the Masson's trichrome-stained sections as the ratio of blue-stained area to total stained area and was calculated using ImageJ software. For the evaluation of neo-epidermal thickness and granular thickness in acute skin wounds, five values were randomly measured in a field and

mean values were calculated using ImageJ software.

2.15 Hemolytic, acute, antimicrobial, and anticoagulant activities of RL-QN15

Both hemolytic activities against human red blood cells and acute toxicity against mice were studied, as described earlier [32]. The antimicrobial activities of RL-QN15 against *E. coli*, *Staphylococcus aureus*, *Bacillus subtilis*, *Streptococcus albicans*, *Staphylococcus haemolyticus* *Candida glabrata*, and *Enterobacter faecalis* were determined according to the previous research [32]. The anticoagulant potential of RL-QN15 against the whole blood of mice was determined following prior research[39].

3. Results

3.1 Purification and determination of amino acid sequences of peptide

The skin secretions of *R. limnocharis* were ultrafiltered and then purified by two rounds of RP-HPLC (Figure S1A and B). One fraction with a retention time of 48 min was purified and showed the ability to accelerate cell scratch healing (data not shown). Mass spectrum analysis indicated that the fraction had a molecular weight of 1 906.71 Da (Figure S2A). DTT treatment increased the molecular weight from 1 906.71 Da to 1 908.69 Da (Figure S2B), indicating the possible existence of a disulfide bridge. The 1 908.69 m/z fragment was then selected as the parent ion for tandem mass spectrometry. Results from b-ions and y-ions suggested that this peptide had an amino acid sequence of 'QNSYAD(I/L)WCQFHYMC' (Figure S2C), which was confirmed as 'QNSYADLWCQFHYMC' by Edman degradation.

3.2 Structural characteristics of peptide

The 'QNSYADLWCQFHYMC' sequence showed no obvious structural similarity with reported peptides in the NCBI database and was thus considered to be novel and named as RL-QN15 accordingly. The RL-QN15 prepropeptide with a 71 amino acid residue length was encoded by a 317-bp cDNA sequence (GenBank accession number: MN722641) (Figure 1A). The theoretical molecular weight was 1 909.14 Da, which showed an increase of ~2 Da from the observed molecular weight of 1 906.71 Da (Figure S2A). Based on these results and the mass spectra of the peptide treated with DTT (Figure S2B), we concluded that an intramolecular disulfide bridge was linked between the 9^{th}C and 15^{th}C. Both the chemical structure and formula of RL-QN15 are displayed in Figure 1B. The advanced structure of RL-QN15 was also predicted, which indicated that the first eight amino acid residues formed an α-helix, followed by a cyclic motif composed of the remaining seven amino acid residues (Figure 1C-F). The prepropeptide of RL-QN15 was similar to that of antimicrobial peptides from other amphibians (Figure S3); however, mature RL-QN15 demonstrated no direct antibacterial activity, hemolytic activity against whole blood cells, or acute toxicity against mice (Table S1-3).

3.3 RL-QN15 promoted full-thickness skin wound healing in mice

A full-thickness dermal skin wound model was established in mice. The regeneration of skin wounds treated with RL-QN15 (50 nM) reached almost 100% on day 7 post-operation. The effect was better than that of the positive control (KFX) and vehicle groups, which only produced a wound healing rate of ~60% (Figure 2A). RL-QN15 showed time-dependent pro-healing activity at concentrations of 1 nM, 10 nM, and 50 nM (Figure 2B). Furthermore, similar

repair-promoting activity was found for 1 nM (2×10^{-6} mg/mL) RL-QN15 and 1 mg/mL KFX, suggesting that RL-QN15 exhibited much greater pro-healing activity (~5×10^{6} times) than that of the commercially used KFX.

Histomorphological analysis was also carried out on skin sections (stained using H&E) from mice on days 5 and 9 post-operation. As shown in Figure 2C, with time, new epidermis and granulation tissue gradually formed in the vehicle group. After local administration of KFX and RL-QN15, the regeneration and reconstruction of the epidermis and granulation tissue were significantly enhanced. In contrast, the new epidermis and granulation tissue thickness in the RL-QN15 and KFX groups was less than that in the vehicle group (Figure 2D). Although there was no notable difference in the thickness of the new epidermis, the thickness of the new granulation tissue in the RL-QN15 group was significantly less than that in the KFX group. Moreover, in the RL-QN15 group, the structures of the damaged dermis and epidermis were very close to that of normal skin, except for the lack of skin appendages, indicating significant potency of RL-QN15 in the acceleration of skin wound healing with little scarring.

3.4 RL-QN15 promoted keratinocyte migration, proliferation, and scratch repair

At concentrations of 100 pM, 1 nM, and 10 nM, RL-QN15 promoted HaCaT cell migration and proliferation in a concentration-dependent manner (Figure 3A-C). As illustrated in Figure 3D, RL-QN15 (10 nM) also markedly promoted HaCaT cell scratch repair at different times (0–24 h). However, the scrambled version of RL-QN15 showed little effect on the restoration of cell scratches. The activity of RL-QN15 in promoting cell scratch repair was concentration- and time-dependent, consistent with the skin repair-promoting activity at the animal level

(Figure 2 and 3E).

3.5 Cell scratch healing activity of RL-QN15 was not dependent on activation of epidermal growth factor receptor (EGFR)

EGFR is an important receptor that meditates epidermal cell scratch repair [40]. As shown in Figure S4, the cell scratch repair rate in the EGFR inhibitor (gefitinib, 1 μM) group was 57.19%, significantly lower than that in the vehicle (75.67%) and 10 nM RL-QN15 groups (88.08%). The repair rate in the gefitinib + RL-QN15 group was 75.49%, which was close to that in the vehicle group, higher than that in the gefitinib group, and lower than that in the RL-QN15 group. Thus, these results indicate that activation of EGFR was not closely related to the cell scratch repair activity of RL-QN15.

3.6 RL-QN15 selectively regulated cytokine release from macrophages

Macrophages participate in the whole process of wound healing, and the cytokines/proteins secreted by macrophages play important roles in the regulation of wound repair [41]. As seen in Figure 4A, at concentrations of 100 pM, 1 nM, and 10 nM, RL-QN15 had no obvious effect on the proliferation of mouse RAW264.7 macrophages, but notably inhibited the release of pro-inflammatory TNF-α induced by LPS (Figure 4B). RL-QN15 also significantly promoted the release of pro-healing TGF-β1 and anti-fibrotic TGF-β3 (Figure 4C and D). In addition, RL-QN15 induced greater release of IL-1β and Smad7 (Figure 4E and F) but had no obvious effect on the release of VEGF or IL-6 (Figure 4G and H). Thus, RL-QN15 showed selective regulation of cytokine release from macrophages.

3.7 MAPK signaling pathway inhibitors blocked RL-QN15-induced release of TGF-β1, but not TGF-β3

Extensive studies have shown that both TGF-β1 and TGF-β3 play important roles in the process of skin repair, with the former promoting healing and the latter inhibiting scar formation. The dynamic regulation of both factors is crucial for wound healing progress [42]. Both the synthesis and release of TGF-β1 are closely related to the MAPK signaling pathway [43]. As shown in Figure S5A, inhibitors of the MAPK signaling pathway, including SP600125 (JNK inhibitor), PD98059 (ERK1/2 inhibitor), and SB203580 (P38 inhibitor), significantly inhibited the release of TGF-β1. As shown in Figure S5B, however, these three inhibitors had no effect on TGF-β3 release. These results suggest that the underlying molecular mechanisms involved in promoting skin-wound healing by RL-QN15 were closely related but not limited to MAPK signaling pathway activation.

3.8 Transcriptome sequencing analysis

We applied transcriptome sequencing to observe the effects of RL-QN15 on the signaling pathways of RAW264.7 cells. As shown in Figure S6A, seven differentially expressed genes (DEGs) were identified between the vehicle and RL-QN15 groups (two up-regulated and five down-regulated). These DEGs were enriched in KEGG pathways related to cellular processes, environmental information processing, and organismal systems (Figure S6B). We identified the top 10 significantly enriched KEGG pathways, which included the MAPK, Toll-like receptor, TNF, IL-17, cAMP, and apoptosis pathways (Figure S6C). GO analysis identified seven DEGs that were primarily related to cellular components, including transcription factor AP-1 complex

(GO: 0035976), nuclear point central transport channel (GO: 0044613), and nuclear outer membrane (GO: 0005640) (Figure S6D).

3.9 RL-QN15 activated MAPK and Smad signaling pathways

As shown in Figure 5A, at concentrations of 100 pM, 1 nM, and 10 nM, RL-QN15 had no effect on total-ERK, JNK, or P38 levels in RAW264.7 cells, consistent with the finding that RL-QN15 did not influence RAW264.7 cell proliferation (Figure 4A), but markedly enhanced the phosphorylation of ERK, JNK, and P38 (Figure 5B, C, and D). The Smad signaling pathway is critical in TGF-β1 signal transduction, with both Smad2 and Smad3 molecules important for downward transmission [43]. As RL-QN15 significantly induced the release of TGF-β1 (Figure 4C), it likely also influenced the Smad signaling pathway. As seen in Figure 6A, RL-QN15 had no obvious effect on the expression levels of total Smad2 and Smad3 in RAW264.7 cells, but significantly increased their phosphorylation levels in a concentration-dependent manner (Figure 6B and C). RL-QN15 also induced higher expression of Smad7 (Figure 6A and D), consistent with the ELISA results (Figure 4F).

Inhibitors of the MAPK signaling pathway (i.e., SP600125 (JNK inhibitor), PD98059 (ERK1/2 inhibitor), and SB203580 (P38 inhibitor)) and TGF-β1/Smad signaling pathway (i.e., ITD-1) significantly blocked RL-QN15 activity related to the migration and scratch-healing of HaCaT and RAW264.7 cells (Figure S7). Thus, the above findings indicate that the effects of RL-QN15 activity on skin cell migration and scratch-healing are closely associated with the MAPK and TGF-β1/Smad signaling pathways.

3.10 RL-QN15 dynamically regulated TGF-β1 and TGF-β3 expression at the animal level

The above results suggest that at the cellular level, RL-QN15 induced the release of TGF-β1 through activation of the MAPK signaling pathway and induced high expression of TGF-β3. Thus, we next detected the effects of RL-QN15 on the expression of these two critical factors in a full-thickness wound model in mice. As illustrated in Figure S8A, no significant changes in the level of TGF-β1 were observed in the vehicle group on days 3 and 9 post-operation. After RL-QN15 (50 nM) was applied locally, the expression of TGF-β1 in wound tissue samples increased significantly in the early stage of wound healing (day 3 post-operation). In contrast, in the late stage of wound repair (day 9 post-operation), RL-QN15 had no effect on the content of TGF-β1 in wound tissue. As shown in Figure S8B, in the vehicle group, the expression of TGF-β3 increased slightly with time (days 3 to 9), and RL-QN15 significantly increased TGF-β3 content in the wound tissue in the early and later stages of wound repair.

3.11 Effects of RL-QN15 on hemostasis in wound repair progress

To explore the molecular mechanism involved in the repair-promoting potency of RL-QN15, we also tested whether RL-QN15 had an effect on the clotting time of whole blood in mice. As shown in Table S4, RL-QN15 had no effect on clotting time, indicating that this peptide had no direct effect on hemostasis during wound repair progress.

3.12 RL-QN15 accelerated healing of chronic wounds induced by diabetes mellitus in mice

To evaluate the therapeutic efficacy of RL-QN15 in chronic skin wound repair, we constructed a diabetes mellitus (DM) mouse model (Table S5). As observed in Figure S9A, the healing of wounds in DM mice was significantly hampered. However, when topically treated with RL-QN15 (50 nM), the healing of chronic wounds significantly increased (Figure S9B).

On day 13 post-injury, wounds were almost completely healed in the RL-QN15-treated group but were only about 50% healed in the vehicle group. Compared with the positive control (exendin-4, 50 nM), RL-QN15 (50 nM) showed parallel pro-healing activity. We also examined the histological thickness of dermal regeneration and granulation on days 5, 9, and 13 post-injury. As shown in Figure S9C, the mice in the vehicle group showed a thickened granulation layer with impaired regeneration in the epidermis, which were both significantly improved by the topical application of RL-QN15.

3.13 RL-QN15 accelerated healing of oral ulcers in rats

As shown in Figure S10A, the topical application of RL-QN15 and KFX (positive control) accelerated the healing of oral ulcers. The recovery of oral ulcers in normal rats required about 12 d. However, this was reduced to less than 7 d when treated with different concentrations of RL-QN15 (1 nM and 10 nM), thus RL-QN15 showed a more potent healing ability than KFX (10 mg/mL) (Figure S10B). The histopathological changes of oral ulcers in rats are shown in Figure S10C. On day 2 post-injury, the formation of an oral ulcer and aggregation of inflammatory cells were observed in the vehicle, KFX, and RL-QN15 groups. With treatment progress, the therapeutic effects of RL-QN15 and KFX became more and more significant, and on day 7 post-injury, the surface of the oral ulcer was completely covered by a new mucosal epithelium and was considered healed. In contrast, obvious oral ulcers with an only partial mucosal epithelium were observed in the vehicle group.

3.14 RL-QN15 significantly ameliorated skin fibrosis in mice

The scarless and accelerated manner in which RL-QN15 repaired skin wounds suggests its

possible application in skin fibrosis treatment. As shown in Figure S11, a subcutaneous injection of RL-QN15 alone showed no obvious effects on dermal thickness or fibrotic level, whereas both were significantly increased by a subcutaneous injection of bleomycin. However, following preventive pretreatment with RL-QN15, the increases in dermal thickness and fibrotic levels induced by bleomycin were obviously ameliorated (Figure S11B and C, respectively). As shown in Figure S12, treatment with RL-QN15 alone had no obvious effects on skin thickness or fibrotic levels, whereas a subcutaneous injection of bleomycin increased both. Following treatment with RL-QN15, the increases in skin thickness and fibrotic levels induced by bleomycin were improved. Thus, these findings highlight the anti-fibrotic effects of RL-QN15 *in vivo*.

4. Discussion

The aim of the current study was to identify novel and potent pro-healing agents. Amphibian skins secrete a diverse range of bioactive peptides with therapeutic potency, which has provoked considerable research attention [27]. Here, a novel short peptide, named RL-QN15, was identified from the skin secretions of *R. limnocharis* frogs. The pro-healing potency of RL-QN15 was demonstrated in mice using full-thickness skin injury models. Compared with several other known pro-healing peptides, such as AH90, tylotoin, temporins, OA-GL21, cathelicidin-OA1, OM-LV20, CW-49, OA-GL12, and OA-FF10 [23, 24, 28, 30, 32, 44, 45], RL-QN15 was one of the shortest peptides, indicating a relatively low cost in its commercial synthesis.

After the development of an acute skin wound, healing follows a set of sequential, yet

overlapping phases, including hemostasis, inflammation, proliferation, and remodeling [3, 46]. Numerous cells, factors, and signaling pathways are activated or inhibited during the different phases of healing [46]. First, our results indicated that RL-QN15 showed no direct effect on hemostasis during wound repair (Table S4). Next, we systematically investigated the underlying mechanisms related to the ability of RL-QN15 to accelerate skin healing.

1) At the cellular level, it is generally accepted that cellular processes, especially migration and proliferation of keratinocytes, fibroblasts, and macrophages, are crucial for the healing of skin wounds [47, 48]. RL-QN15 markedly induced keratinocyte migration and proliferation and thus promoted the healing of cell scratch injuries (Figure 3), although this activity showed little relevance to EGFR activation (Figure S4).

2) Macrophages play core roles at almost every stage of wound healing, such as recruiting other cells to the wound site and inducing cell proliferation and tissue remodeling. Macrophages also produce many cytokines associated with wound healing, such as TNF-α, IL-6, TGF-β1, VEGF, and TGF-β3 [42, 48, 49]. Here, RL-QN15 significantly blocked the release of proinflammatory TNF-α induced by LPS challenge and induced the release of proinflammatory IL-1β but not IL-6 (Figure 4). These results highlight the highly complex mechanisms involved in the repair-promoting ability of RL-QN15 in regard to inflammation. In the early stage of inflammation, proinflammatory cytokines, such as TNF-α, IL-6, and IL-1β, recruit other inflammatory cells to secrete pro-healing growth factors to modify the migration and proliferation of cells closely related to wound repair [42, 50]. Thus, it is reasonable to speculate that the release of proinflammatory IL-1β induced by RL-QN15 may be beneficial for its pro-

healing potency by inducing inflammation and hence recruiting additional macrophages to the wound site. However, an excessive inflammatory response is harmful to wound repair and can lead to scar formation [41, 51]. Thus, the inhibitory effects of RL-QN15 against the release of TNF-α may also contribute to its pro-healing potency and limited scarring (Figure 2C and D). RL-QN15 also induced the synthesis of Smad7 (Figure 4E, Figure 6A and D), which may provide further clues to the scarless pro-healing potency of RL-QN15 at wound sites [52, 53].

During wound healing, TGF-β1 is important in inflammation, angiogenesis, re-epithelialization, and connective tissue regeneration [43, 54, 55]. Furthermore, TGF-β1 helps monocytes convert to macrophages, which initiate the development of granulation tissue and the release of a variety of cytokines and growth factors that contribute to wound repair [55, 56]. However, it has been proposed that high levels of TGF-β1 can also contribute to skin fibrosis, which is closely related to the formation of scars in adults. In contrast, isoform TGF-β3 is suggested to have an antifibrotic effect during wound healing [56-58]. We found that RL-QN15 induced the release of TGF-β1 (Figure 4C) and TGF-β3 (Figure 4D) from macrophages. As shown in Figure S7, in the early stages of wound healing, RL-QN15 treatment induced a significant increase in the levels of both TGF-β1 and TGF-β3; in the later stages, however, RL-QN15 showed no effect on the level of TGF-β1 but induced greater expression of TGF-β3. Thus, we assumed that RL-QN15 subtly altered the ratio of TGF-β1 and TGF-β3 during adult wound repair, thereby inducing more rapid wound healing and less scar formation.

3) Wound healing is one of the most complex processes in multicellular organisms, involving numerous signaling pathways and various cell types [6, 47, 59]. MAPK signaling has

been implicated in the regulation of TGF-β production and release from skin cells and plays an important role in wound healing [60]. Here, western blot analysis showed that RL-QN15 significantly increased the activation of ERK, JNK, and P38 in the MAPK signaling pathway (Figure 5). Specific inhibitors of ERK, JNK, and P38 blocked the up-regulation of TGF-β1 induced by RL-QN15 (Figure S5), suggesting that these kinases are involved in RL-QN15-induced TGF-β1 secretion. To further demonstrate that RL-QN15 up-regulated TGF-β1, we investigated the effects of RL-QN15 on Smad2 and Smad3, which are essential components of downstream TGF-β signaling [43]. As illustrated in Figure 6, RL-QN15 significantly activated the phosphorylation of Smad2 and Smad3. As shown in Figure S7, the action of RL-QN15 on skin cell migration and scratch healing was closely related to the TGF-β1/Smad signaling pathway. The transcriptome sequencing results also implied that in addition to MAPK, many other signaling pathways, including IL-17, Toll-like receptor, and TNF, may be closely related to the pro-healing mechanisms of RL-QN15 (Figure S6). However, further detailed research is required to clarify these results.

It should be noted that poor pharmacokinetics pose a significant obstacle for the clinical translation of peptides, even when topical applications are envisaged. Peptides are easily modified by endogenous (e.g., tyrosinase, elastase, metalloproteinase) and exogenous (e.g., produced by colonized microorganisms) enzymes at the wound site [50, 61]. Therefore, it is of utmost importance to evaluate the tolerance of RL-QN15 to enzymes in further studies.

In summary, we identified a short pro-healing peptide (RL-QN15) from the skin secretions of *R. limnocharis* and highlighted RL-QN15 as a potential candidate for the novel development

of pro-healing agents.

5. Conclusions

Our results highlight the potential of frog skin secretions as a treasure trove of bioactive peptides. Furthermore, the novel peptide (RL-QN15) identified in this research demonstrates considerable potential as a candidate for the development of novel pro-healing agents.

Authors' contributions

Conception and design: Xinwang Yang, Jing Tang, and Ying Wang; Research and acquisition of data: Ying Wang, Zhuo Feng, Meifeng Yang, Lin Zeng, Bu'er Qi, Saige Yin, Bangsheng Li, Yilin Li, Longjun Shu, Chen Fu, Pan Qin, and Yi Meng; Analysis and interpretation of data: Ying Wang, Zhuo Feng, Meifeng Yang, Lin Zeng, Bu'er Qi, Saige Yin, Bangsheng Li, Yilin Li, Longjun Shu, Chen Fu, Pan Qin, Yi Meng, Xiaojie Li, Ying Yang, Jing Tang, and Xinwang Yang; Writing and review of the manuscript: Xinwang Yang, Jing Tang, and Ying Wang; Study supervision: Xinwang Yang.

CONFLICT OF INTEREST

The authors declare no competing financial interest

Declaration Sections

Ethics approval and consent to participate

All animal procedures were approved and conducted in accordance with the requirements of the Ethics Committee of Kunming Medical University (KMMU20180012).

Consent for publication

Not applicable.

Availability of data and materials

The datasets in the current study are available from the corresponding author on reasonable request.

Competing interests

The authors state no conflict of interest.

Funding

This work was supported by grants from the National Natural Science Foundation of China (81760648, 31660244, 32060212, and 31670776), Yunnan Applied Basic Research Project Foundation (2019FB128), Yunnan Applied Basic Research Project Foundation-Kunming Medical University Union Foundation (2019FE001 (-019) and 2019FE001 (-020)), Endocrine Clinical Medical Center (ZX2019‐02‐02), and Diabetic Innovation Team (2019HC002) of Yunnan Province.

Acknowledgements

Not applicable.

References

[1] P. Martin, Wound healing--aiming for perfect skin regeneration, Science 276(5309) (1997) 75-81.

[2] M. Takeo, W. Lee, M. Ito, Wound healing and skin regeneration, Cold Spring Harb Perspect Med 5(1) (2015) a023267.

[3] A. Kasuya, Y. Tokura, Attempts to accelerate wound healing, J Dermatol Sci 76(3) (2014) 169-72.

[4] E.A. Gantwerker, D.B. Hom, Skin: histology and physiology of wound healing, Clin Plast Surg 39(1) (2012) 85-97.

[5] P. Martin, R. Nunan, Cellular and molecular mechanisms of repair in acute and chronic wound healing, Br J Dermatol 173(2) (2015) 370-8.

[6] P.H. Wang, B.S. Huang, H.C. Horng, C.C. Yeh, Y.J. Chen, Wound healing, J Chin Med Assoc 81(2) (2018) 94-101.

[7] D.G. Armstrong, A.J.M. Boulton, S.A. Bus, Diabetic Foot Ulcers and Their Recurrence, N Engl J Med 376(24) (2017) 2367-2375.

[8] G. Han, R. Ceilley, Chronic Wound Healing: A Review of Current Management and Treatments, Adv Ther 34(3) (2017) 599-610.

[9] T. Leavitt, M.S. Hu, C.D. Marshall, L.A. Barnes, H.P. Lorenz, M.T. Longaker, Scarless wound healing: finding the right cells and signals, Cell Tissue Res 365(3) (2016) 483-93.

[10] S.R. Park, J.W. Kim, H.S. Jun, J.Y. Roh, H.Y. Lee, I.S. Hong, Stem Cell Secretome and Its Effect on Cellular Mechanisms Relevant to Wound Healing, Mol Ther 26(2) (2018) 606-617.

[11] D. Comegna, A. Zannetti, A. Del Gatto, I. de Paola, L. Russo, S. Di Gaetano, A. Liguoro,

D. Capasso, M. Saviano, L. Zaccaro, Chemical Modification for Proteolytic Stabilization of the Selective alphavbeta3 Integrin RGDechi Peptide: in Vitro and in Vivo Activities on Malignant Melanoma Cells, J Med Chem 60(23) (2017) 9874-9884.

[12] T.T. Nguyen, D. Ding, W.R. Wolter, R.L. Perez, M.M. Champion, K.V. Mahasenan, D. Hesek, M. Lee, V.A. Schroeder, J.I. Jones, E. Lastochkin, M.K. Rose, C.E. Peterson, M.A. Suckow, S. Mobashery, M. Chang, Validation of Matrix Metalloproteinase-9 (MMP-9) as a Novel Target for Treatment of Diabetic Foot Ulcers in Humans and Discovery of a Potent and Selective Small-Molecule MMP-9 Inhibitor That Accelerates Healing, J Med Chem 61(19) (2018) 8825-8837.

[13] T.V.A. Lordani, C.E. de Lara, F.B.P. Ferreira, M. de Souza Terron Monich, C. Mesquita da Silva, C.R. Felicetti Lordani, F. Giacomini Bueno, J.J. Vieira Teixeira, M.V.C. Lonardoni, Therapeutic Effects of Medicinal Plants on Cutaneous Wound Healing in Humans: A Systematic Review, Mediators Inflamm 2018 (2018) 7354250.

[14] T. Maver, U. Maver, K. Stana Kleinschek, D.M. Smrke, S. Kreft, A review of herbal medicines in wound healing, Int J Dermatol 54(7) (2015) 740-51.

[15] T. Dinh, S. Braunagel, B.I. Rosenblum, Growth factors in wound healing: the present and the future?, Clin Podiatr Med Surg 32(1) (2015) 109-19.

[16] Y. Zhang, Why do we study animal toxins?, Dongwuxue Yanjiu 36(4) (2015) 183-222.

[17] A.A. Kaspar, J.M. Reichert, Future directions for peptide therapeutics development, Drug Discov Today 18(17-18) (2013) 807-17.

[18] K. Fosgerau, T. Hoffmann, Peptide therapeutics: current status and future directions, Drug Discov Today 20(1) (2015) 122-8.

[19] J.L. Lau, M.K. Dunn, Therapeutic peptides: Historical perspectives, current development trends, and future directions, Bioorg Med Chem 26(10) (2018) 2700-2707.

[20] A. Henninot, J.C. Collins, J.M. Nuss, The Current State of Peptide Drug Discovery: Back to the Future?, J Med Chem 61(4) (2018) 1382-1414.

[21] X. Yang, Y. Wang, C. Wu, E.A. Ling, Animal Venom Peptides as a Treasure Trove for New Therapeutics Against Neurodegenerative Disorders, Curr Med Chem 26(25) (2019) 4749-4774.

[22] Z. Yan, S. Zhu, H. Wang, L. Wang, T. Du, Z. Ye, D. Zhai, Z. Zhu, X. Tian, Z. Lu, X. Cao, MOTS-c inhibits Osteolysis in the Mouse Calvaria by affecting osteocyte-osteoclast crosstalk and inhibiting inflammation, Pharmacol Res 147 (2019) 104381.

[23] I. Demori, Z.E. Rashed, V. Corradino, A. Catalano, L. Rovegno, L. Queirolo, S. Salvidio, E. Biggi, M. Zanotti-Russo, L. Canesi, A. Catenazzi, E. Grasselli, Peptides for Skin Protection and Healing in Amphibians, Molecules 24(2) (2019).

[24] A. Di Grazia, V. Luca, L.A. Segev-Zarko, Y. Shai, M.L. Mangoni, Temporins A and B stimulate migration of HaCaT keratinocytes and kill intracellular Staphylococcus aureus, Antimicrob Agents Chemother 58(5) (2014) 2520-7.

[25] A. Di Grazia, F. Cappiello, A. Imanishi, A. Mastrofrancesco, M. Picardo, R. Paus, M.L. Mangoni, The Frog Skin-Derived Antimicrobial Peptide Esculentin-1a(1-21)NH2 Promotes the Migration of Human HaCaT Keratinocytes in an EGF Receptor-Dependent Manner: A Novel Promoter of Human Skin Wound Healing?, PLoS One 10(6) (2015) e0128663.

[26] A. Di Grazia, F. Cappiello, H. Cohen, B. Casciaro, V. Luca, A. Pini, Y.P. Di, Y. Shai, M.L. Mangoni, D-Amino acids incorporation in the frog skin-derived peptide esculentin-1a(1-21)NH2 is beneficial for its multiple functions, Amino Acids 47(12) (2015) 2505-19.

[27] X. Yang, W.H. Lee, Y. Zhang, Extremely abundant antimicrobial peptides existed in the skins of nine kinds of Chinese odorous frogs, J Proteome Res 11(1) (2012) 306-19.

[28] Y. Song, C. Wu, X. Zhang, W. Bian, N. Liu, S. Yin, M. Yang, M. Luo, J. Tang, X. Yang, A short peptide potentially promotes the healing of skin wound, Biosci Rep 39(3) (2019).

[29] Y. Shen, J. Maupetit, P. Derreumaux, P. Tuffery, Improved PEP-FOLD Approach for Peptide and Miniprotein Structure Prediction, J Chem Theory Comput 10(10) (2014) 4745-58.

[30] X. Li, Y. Wang, Z. Zou, M. Yang, C. Wu, Y. Su, J. Tang, X. Yang, OM-LV20, a novel peptide from odorous frog skin, accelerates wound healing in vitro and in vivo, Chem Biol Drug Des 91(1) (2018) 126-136.

[31] Y. Song, C. Wu, X. Zhang, W. Bian, N. Liu, S. Yin, M. Yang, M. Luo, J. Tang, X. Yang, A short peptide potentially promotes the healing of skin wound, Biosci Rep (2019).

[32] X. Cao, Y. Wang, C. Wu, X. Li, Z. Fu, M. Yang, W. Bian, S. Wang, Y. Song, J. Tang, X. Yang, Cathelicidin-OA1, a novel antioxidant peptide identified from an amphibian, accelerates skin wound healing, Sci Rep 8(1) (2018) 943.

[33] G. Roy Choudhury, M.G. Ryou, E. Poteet, Y. Wen, R. He, F. Sun, F. Yuan, K. Jin, S.H. Yang, Involvement of p38 MAPK in reactive astrogliosis induced by ischemic stroke, Brain Res 1551 (2014) 45-58.

[34] X. Wang, W. Zou, H. Yu, Y. Lin, G. Dai, T. Zhang, G. Zhang, K. Xie, J. Wang, H. Shi, RNA Sequencing Analysis of Chicken Cecum Tissues Following Eimeria tenella Infection in Vivo, Genes (Basel) 10(6) (2019).

[35] S. Yin, Y. Wang, N. Liu, M. Yang, Y. Hu, X. Li, Y. Fu, M. Luo, J. Sun, X. Yang, Potential skin protective effects after UVB irradiation afforded by an antioxidant peptide from Odorrana

andersonii, Biomed Pharmacother 120 (2019) 109535.

[36] J.N. Roan, H.N. Cheng, C.C. Young, C.J. Lee, M.L. Yeh, C.Y. Luo, Y.S. Tsai, C.F. Lam, Exendin-4, a glucagon-like peptide-1 analogue, accelerates diabetic wound healing, J Surg Res 208 (2017) 93-103.

[37] Y.S. Lim, S.K. Kwon, J.H. Park, C.G. Cho, S.W. Park, W.K. Kim, Enhanced mucosal healing with curcumin in animal oral ulcer model, The Laryngoscope 126(2) (2016) E68-73.

[38] V.H. Luong, T. Chino, N. Oyama, T. Matsushita, Y. Sasaki, D. Ogura, S.I. Niwa, T. Biswas, A. Hamasaki, M. Fujita, Y. Okamoto, M. Otsuka, H. Ihn, M. Hasegawa, Blockade of TGF-beta/Smad signaling by the small compound HPH-15 ameliorates experimental skin fibrosis, Arthritis Res Ther 20(1) (2018) 46.

[39] A.R. Arenajo, A.P. Ybanez, M.M.P. Ababan, C.E. Villajuan, M.R.M. Lasam, C.P. Young, J.L.A. Reyes, The potential anticoagulant property of Caulerpa lentillifera crude extract, International journal of health sciences 11(3) (2017) 29-32.

[40] M.R. Schneider, S. Werner, R. Paus, E. Wolf, Beyond wavy hairs: the epidermal growth factor receptor and its ligands in skin biology and pathology, Am J Pathol 173(1) (2008) 14-24.

[41] S.A. Eming, T. Krieg, J.M. Davidson, Inflammation in wound repair: molecular and cellular mechanisms, J Invest Dermatol 127(3) (2007) 514-25.

[42] S. Werner, R. Grose, Regulation of wound healing by growth factors and cytokines, Physiol Rev 83(3) (2003) 835-70.

[43] L. Mu, J. Tang, H. Liu, C. Shen, M. Rong, Z. Zhang, R. Lai, A potential wound-healing-promoting peptide from salamander skin, FASEB J 28(9) (2014) 3919-29.

[44] N. Liu, Z. Li, B. Meng, W. Bian, X. Li, S. Wang, X. Cao, Y. Song, M. Yang, Y. Wang, J.

Tang, X. Yang, Accelerated wound healing induced by a novel amphibian peptide (OA-FF10), Protein Pept Lett (2019).

[45] W. Bian, B. Meng, X. Li, S. Wang, X. Cao, N. Liu, M. Yang, J. Tang, Y. Wang, X. Yang, OA-GL21, a novel bioactive peptide from Odorrana andersonii, accelerated the healing of skin wounds, Biosci Rep 38(3) (2018).

[46] S.A. Eming, P. Martin, M. Tomic-Canic, Wound repair and regeneration: mechanisms, signaling, and translation, Sci Transl Med 6(265) (2014) 265sr6.

[47] M.C. Heng, Wound healing in adult skin: aiming for perfect regeneration, Int J Dermatol 50(9) (2011) 1058-66.

[48] M. Peiseler, P. Kubes, Macrophages play an essential role in trauma-induced sterile inflammation and tissue repair, Eur J Trauma Emerg Surg 44(3) (2018) 335-349.

[49] S. Barrientos, H. Brem, O. Stojadinovic, M. Tomic-Canic, Clinical application of growth factors and cytokines in wound healing, Wound Repair Regen 22(5) (2014) 569-78.

[50] N. Kumar, C. Yin, The anti-inflammatory peptide Ac-SDKP: Synthesis, role in ACE inhibition, and its therapeutic potential in hypertension and cardiovascular diseases, Pharmacol Res 134 (2018) 268-279.

[51] S.M. Karppinen, R. Heljasvaara, D. Gullberg, K. Tasanen, T. Pihlajaniemi, Toward understanding scarless skin wound healing and pathological scarring, F1000Res 8 (2019).

[52] G. Han, F. Li, P. Ten Dijke, X.J. Wang, Temporal smad7 transgene induction in mouse epidermis accelerates skin wound healing, Am J Pathol 179(4) (2011) 1768-79.

[53] C.L. Gallant-Behm, T.A. Mustoe, Occlusion regulates epidermal cytokine production and inhibits scar formation, Wound Repair Regen 18(2) (2010) 235-44.

[54] S. Barrientos, O. Stojadinovic, M.S. Golinko, H. Brem, M. Tomic-Canic, Growth factors and cytokines in wound healing, Wound Repair Regen 16(5) (2008) 585-601.

[55] M. Morikawa, R. Derynck, K. Miyazono, TGF-beta and the TGF-beta Family: Context-Dependent Roles in Cell and Tissue Physiology, Cold Spring Harb Perspect Biol 8(5) (2016).

[56] M.K. Lichtman, M. Otero-Vinas, V. Falanga, Transforming growth factor beta (TGF-beta) isoforms in wound healing and fibrosis, Wound Repair Regen 24(2) (2016) 215-22.

[57] L. Wang, J. Yang, B. Ran, X. Yang, W. Zheng, Y. Long, X. Jiang, Small Molecular TGF-beta1-Inhibitor-Loaded Electrospun Fibrous Scaffolds for Preventing Hypertrophic Scars, ACS Appl Mater Interfaces 9(38) (2017) 32545-32553.

[58] M. Le, R. Naridze, J. Morrison, L.C. Biggs, L. Rhea, B.C. Schutte, V. Kaartinen, M. Dunnwald, Transforming growth factor Beta 3 is required for excisional wound repair in vivo, PLoS One 7(10) (2012) e48040.

[59] A.V. Ljubimov, M. Saghizadeh, Progress in corneal wound healing, Prog Retin Eye Res 49 (2015) 17-45.

[60] J.C. Lee, J.T. Laydon, P.C. McDonnell, T.F. Gallagher, S. Kumar, D. Green, D. McNulty, M.J. Blumenthal, J.R. Heys, S.W. Landvatter, J.E. Strickler, M.M. McLaughlin, I.R. Siemens, S.M. Fisher, G.P. Livi, J.R. White, J.L. Adams, P.R. Young, A protein kinase involved in the regulation of inflammatory cytokine biosynthesis, Nature 372(6508) (1994) 739-46.

[61] R. Smits, B. Koksch, How C(alpha)-Fluoroalkyl amino acids and peptides interact with enzymes: studies concerning the influence on proteolytic stability, enzymatic resolution and peptide coupling, Curr Top Med Chem 6(14) (2006) 1483-98.

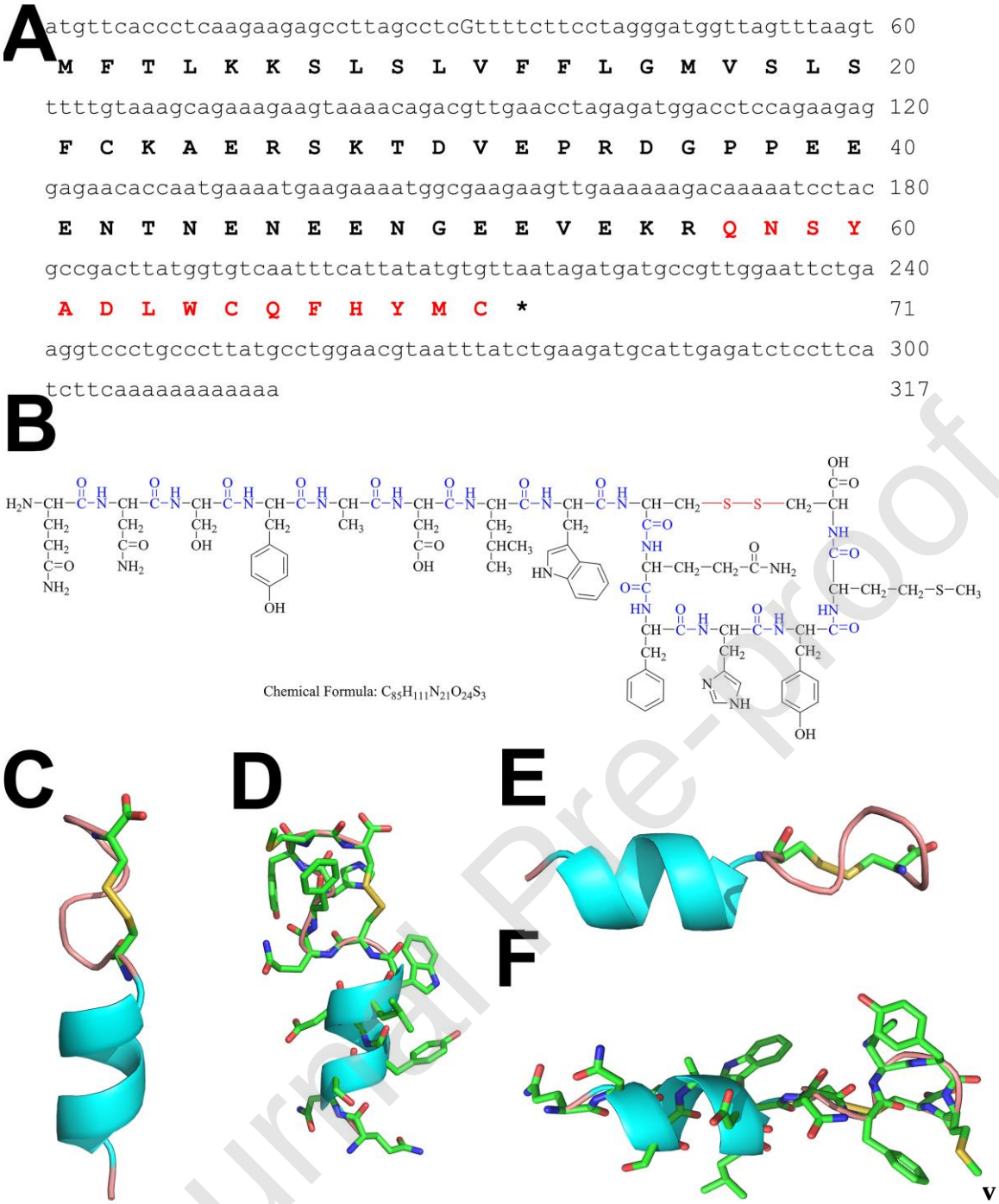

Figure 1. Structural characteristics of RL-QN15.

A. Prepropeptide of RL-QN15 composed of a 71 amino-acid residue encoded by 317-bp cDNA. Mature sequence of RL-QN15 is shown in red, with an intramolecular disulfide bridge located between 9thC and 15thC.

B. Chemical structure of RL-QN15 (drawn by ChemDraw®), with chemical formula of $C_{85}H_{111}N_{21}O_{24}S_3$. Peptide bonds are shown in blue and disulfide bridge is shown in red.

C-F. Different views of advanced structure of RL-QN15 predicted by PEP-FOLD3. Blue: nitrogen atoms, Red: oxygen atoms, Yellow: sulfur atoms, Light Red: disulfide bridge, Blue-green: α-helix.

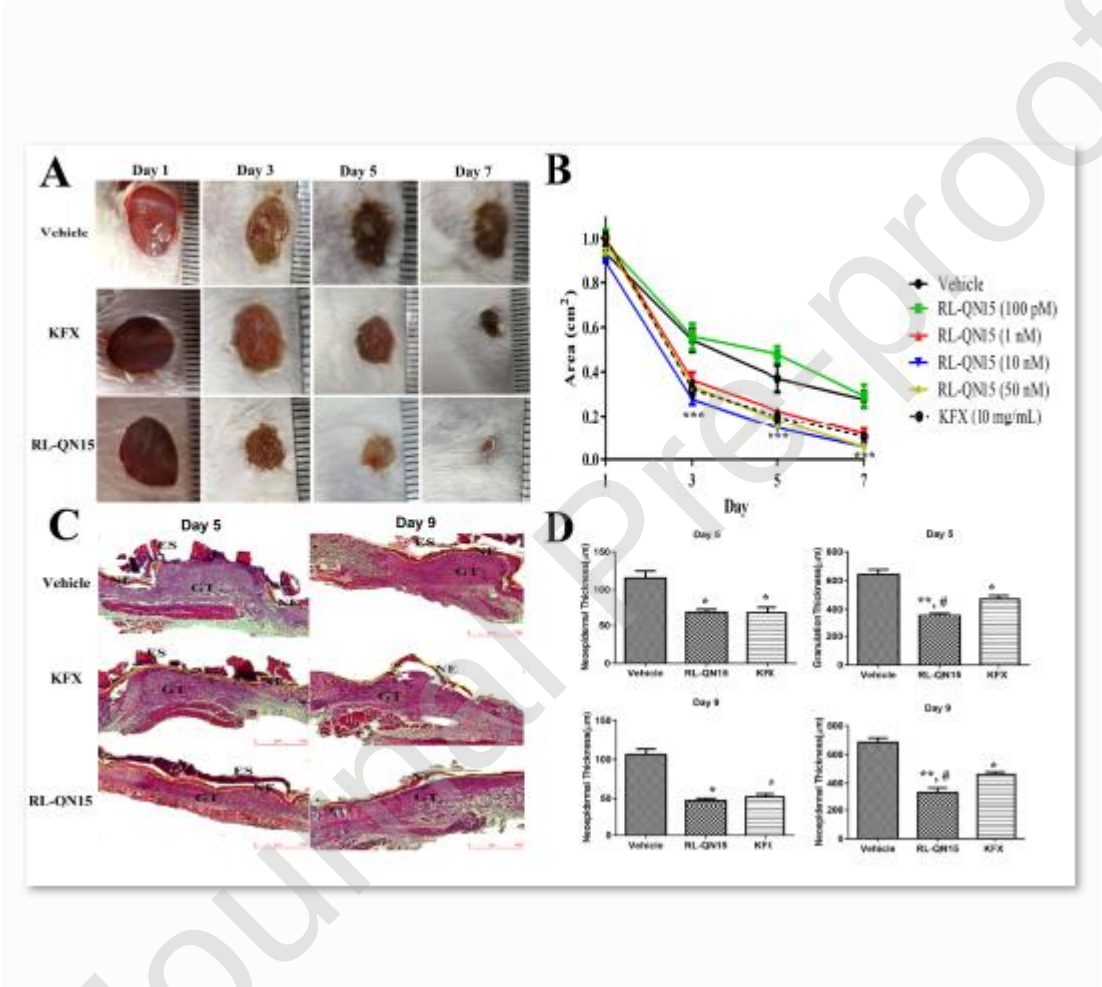

Figure 2. Topical application of RL-QN15 accelerated healing of full-thickness skin wounds in mice.

A. Representative images of skin wounds on days 1, 3, 5, and 7 post-injury in vehicle, KFX-, and RL-QN15-treated groups. KFX (10 mg/mL) and RL-QN15 (50 nM) were applied topically

twice a day to skin wounds.

B. Quantitative curves of pro-healing activities of RL-QN15 at concentrations of 100 pM, 1 nM, 10 nM, and 50 nM. ***$P < 0.0001$ indicates statistically significant differences compared to vehicle group.

C. Representative images of skin wound sections stained with H&E indicating histomorphological changes in skin wounds on days 5 and 9 post-injury in vehicle-, KFX (10 mg/mL)-, and RL-QN15 (50 nM)-treated groups. Yellow line indicates neoepithelium. NE: Neoepithelium; GT: Granular tissue, ES: Eschar. Scale bar is indicated by red line in left lower corner of images.

D. Histological thickness of neoepidermal regeneration and granulation on days 5 and 9 post-injury. *$P < 0.05$, **$P < 0.01$ indicate statistically significant differences compared with vehicle group and $^{\#}P < 0.05$ indicates statistically significant differences compared with KFX group.

Saline was used as the vehicle. Values are expressed as means ± SEM from 6 mice (n = 6).

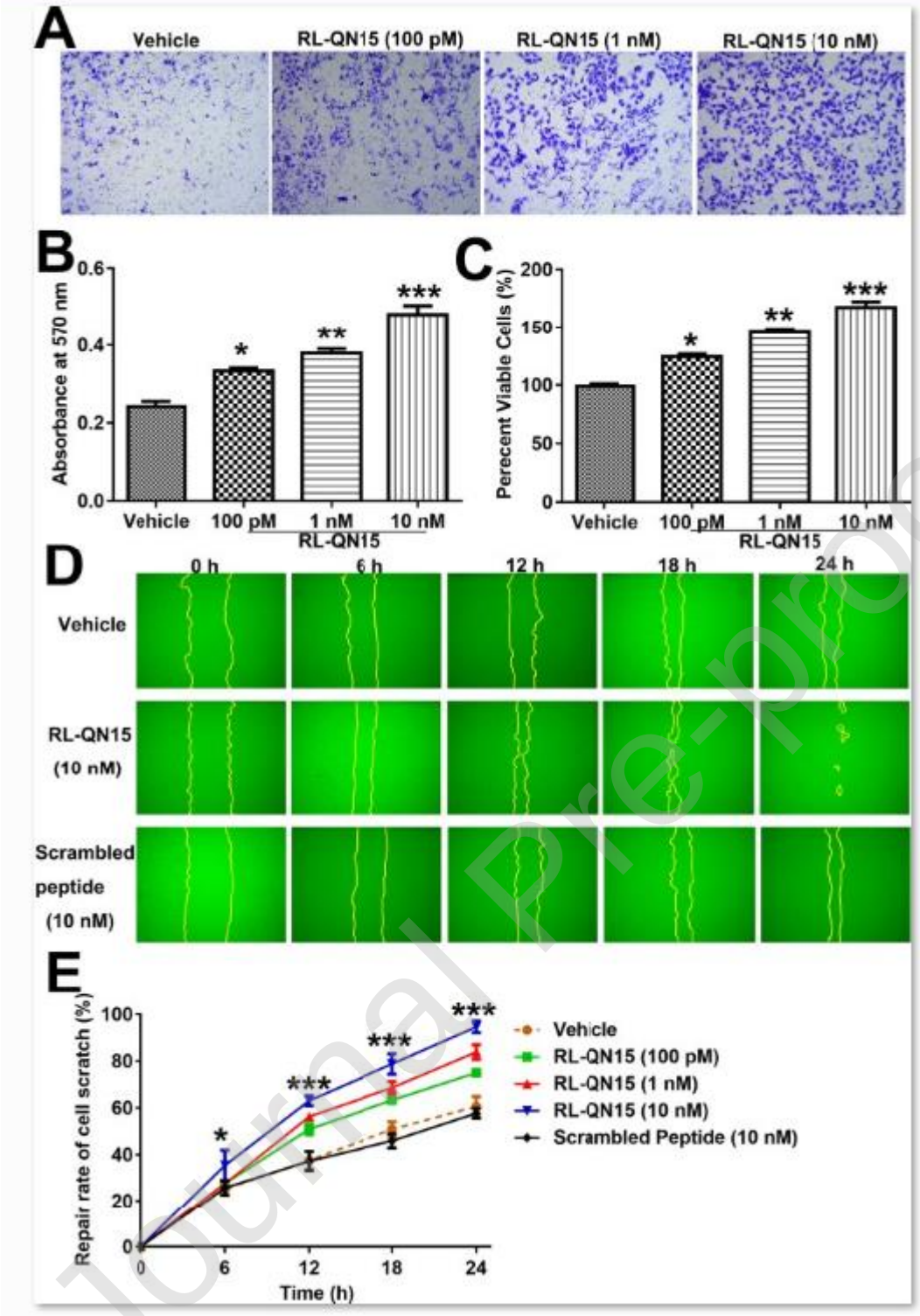

Figure 3. Effects of RL-QN15 on migration, proliferation, and scratch healing of keratinocytes.

A. Representative images displaying migration-promoting activity of RL-QN15 (100 pM, 1 nM,

and 10 nM) against HaCaT cells.

B. Quantitative illustration of concentration-dependent migration-promoting capacity of RL-QN15 against HaCaT cells.

C. Quantitative pro-proliferative effects of RL-QN15 (100 pM, 1 nM, and 10 nM) against HaCaT cells.

D. Representative images displaying effects of vehicle (saline), RL-QN15 (10 nM), and scrambled-control of RL-QN15 (10 nM) on healing of HaCaT cell scratches.

E. Quantitative curves showing concentration- and time-dependent capacity of RL-QN15 at promoting cell scratch healing.

Values are expressed as means ± SEM of six independent experiments performed in triplicate, error bars represent SEM. *$P < 0.05$, **$P < 0.01$, and ***$P < 0.0001$ indicate statistically significant differences compared to vehicle.

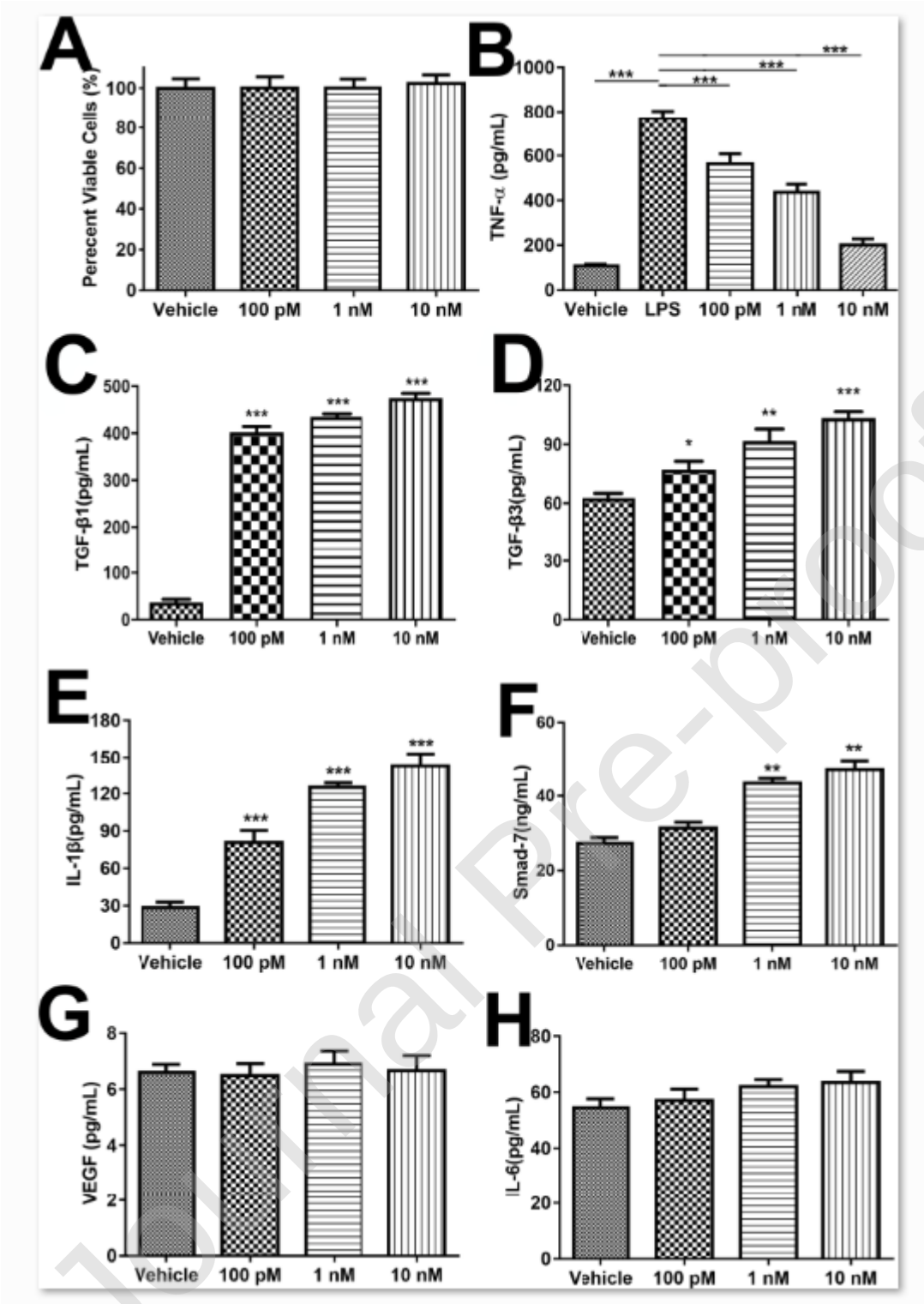

Figure 4. Effects of RL-QN15 on levels of cytokines/proteins secreted by macrophages.

A. Effects of RL-QN15 on proliferation of RAW264.7 cells.

B. Effects of RL-QN15 on release of TNF-α from RAW264.7 cells. RAW264.7 cells were

stimulated by LPS (1 μg/mL) alone or in combination with RL-QN15.

C-H. Effects of RL-QN15 on release of TGF-β1, TGF-β3, IL-1β, Smad7, VEGF, and IL-6, respectively.

Values are expressed as means ± SEM of six independent experiments performed in triplicate. For C-H, $*P < 0.05$, $**P < 0.01$, and $***P < 0.0001$ indicate statistically significant differences compared to vehicle. For B, $*P < 0.05$, $**P < 0.01$, and $***P < 0.0001$ indicate statistically significant differences between two groups.

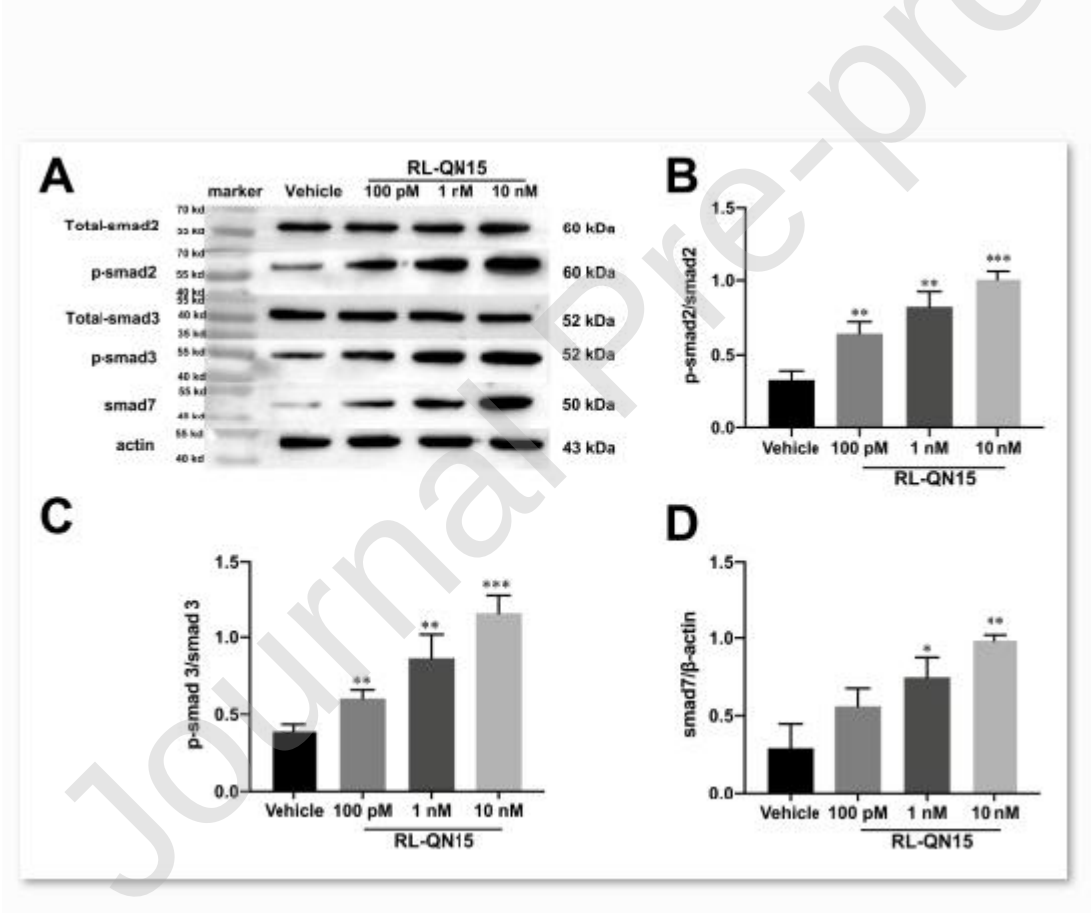

Figure 5. Effects of RL-QN15 on MAPK signaling pathways.

A. Representative western blot images displaying effects of RL-QN15 on expression and

phosphorylation levels of protein kinases ERK, JNK, and P38.

B-D. Quantitative phosphorylation levels compared with total expression levels of ERK, JNK, and P38.

Values are expressed as means ± SEM (n = 3). *P < 0.05, **P < 0.01, and ***P < 0.0001 indicate statistically different from vehicle.

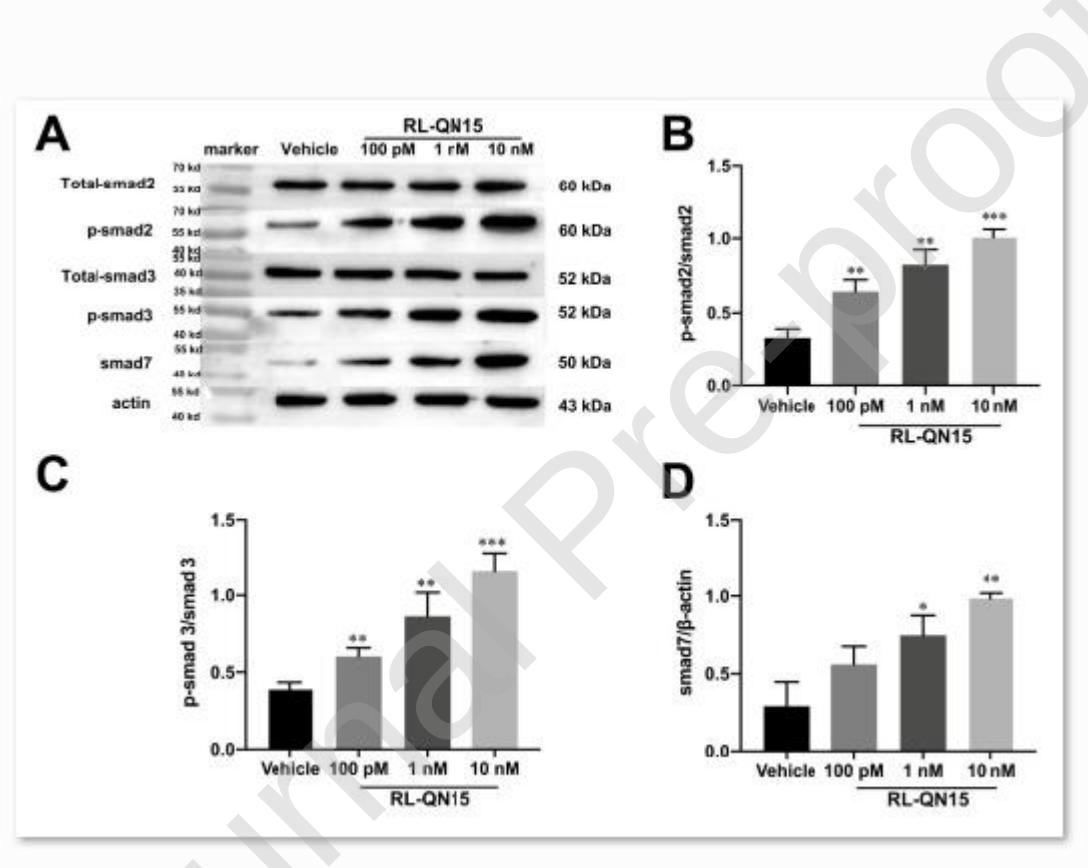

Figure 6. Effects of RL-QN15 on Smad signaling pathway.

A. Representative western blot images displaying effects of RL-QN15 on expression and phosphorylation levels of Smad2 and Smad3 and expression level of Smad7.

B-C. Quantitative phosphorylation levels compared with total expression levels of Smad2 and

Smad3.

D. Quantitative expression level of Smad7 compared with actin.

Values are expressed as means ± SEM (n = 3). *P < 0.05, **P < 0.01, and ***P < 0.0001 indicate statistically different from vehicle.

Table 1

	Chow	Chow/50C	HFD	HFD/50C	HFD/100C	DIO	DIO/50C
Glucose (mg/dl)	**121.03 ± 6.54**	**96.46 ± 1.64**	**166.36 ± 8.69***	**129.52 ± 7.81 †**	**132.42 ± 9.57 †**	**165.78 ± 8.88**	**113.50 ± 2.00 ‡**
Total Cholesterol (mg/dl)	**120.29 ± 8.50**	**109.33 ± 11.29**	**228.68 ± 7.83***	**200.00 ± 5.24 †**	**178.00 ± 13.70 †**	**220.29 ± 6.47**	**182.00 ± 7.04 ‡**
LDL-C (mg/dl)	**32.76 ± 2.31**	**29.78 ± 2.11**	**66.67 ± 1.72***	**49.78 ± 4.65 †**	**54.22 ± 3.93 †**	**62.10 ± 2.90**	**53.87 ± 3.42 ‡**
HDL-C (mg/dl)	**87.52 ± 7.64**	**79.56 ± 10.44**	**162.00 ± 8.07***	**150.22 ± 9.35 †**	**123.78 ± 10.12 †**	**158.19 ± 4.32**	**128.13 ± 7.10**
Triglyceride (mg/dl)	**57.14 ± 5.31**	**53.41 ± 2.74**	**99.24 ± 3.67***	**84.09 ± 2.87 †**	**76.82 ± 9.59 †**	**100.85 ± 5.83**	**76.82 ± 8.78 ‡**
ALT (U/L)	**27.21 ± 7.61**	**27.94 ± 1.95**	**48.54 ± 7.49***	**23.02 ± 4.86 †**	**32.85 ± 3.21 †**	**39.33 ± 3.45**	**27.75 ± 1.81 ‡**